

Ballistic transport: A view from the quantum theory of motion

Hua Wu and D. W. L. Sprung

Department of Physics and Astronomy, McMaster University

Hamilton, Ontario L8S 4M1 Canada

(Submitted to Phys. Lett. A on April 1994)

Abstract

Ballistic transport of electrons through a quantum wire with a constriction is studied in terms of Bohm's interpretation of quantum mechanics, in which the concept of a particle orbit is permitted. The classical bouncing ball trajectories, which justify the name "ballistic transport", are established in the large wave number limit. The formation and the vital role of quantum vortices is investigated.

03.65.Sq, 72.10-d, 47.32.Cc

arXiv:cond-mat/9408063v1 19 Aug 1994

The ballistic transport of electrons in quantum devices based on the two-dimensional electron gas is a subject of intense study. The name “ballistic transport” is borrowed from classical mechanics where a point-like particle moves freely in a region except for elastic collisions with obstacles or the confining walls. Obviously, the classical orbits are straight line segments connected through a reflection law. Quantum devices based on ballistic transport can be approximately thought of as an electron waveguide, in which the electrons behave as non-interacting particles of effective mass m^* in a constant potential with hard wall confinement. While the picture of bouncing balls is a vivid one, quantum mechanically we need a precise justification for this picture. For this purpose, we study here a very simple model, that of a quantum wire with a constriction, to see how classical orbits emerge from the quantum wavefunction.

We consider a straight quantum wire of width d . At the origin $x = 0$ we place a thin but opaque obstacle attached to one side wall so that the channel opening is narrowed to a . Electrons of energy E are injected from the left in transverse mode n_i . In order to develop our argument, we solve this problem by the mode matching method.

Denote the wavefunction to the left and right of the narrow constriction as Ψ_1 and Ψ_2 respectively. These can be expanded in plane waves as

$$\Psi_\Gamma = \sum_n (C_{\Gamma n} e^{i\alpha_n x} + \bar{C}_{\Gamma n} e^{-i\alpha_n x}) \sin(k_n y) \quad (1)$$

where $\Gamma = 1, 2$, $k_n = n\pi/d$, and

$$\alpha_n = \sqrt{E - k_n^2} \quad (2)$$

with appropriate units such that $\hbar^2/(2m^*) = 1$. We also define symbols $C_{\Gamma n}^\pm = C_{\Gamma n} \pm \bar{C}_{\Gamma n}$. At $x = 0$, the wavefunction in the opening is expanded as

$$\text{sn}(y) \equiv \Psi|_{x=0} = \begin{cases} \sum_m D_m \sin \frac{m\pi y}{a} & 0 < y < a \\ 0 & a < y < d \end{cases} \quad (3)$$

Continuity of the wavefunction at $x = 0$ requires that

$$C_{1n}^+ = C_{2n}^+ = \sum_m I_{nm} D_m \quad (4)$$

where

$$\begin{aligned} I_{nm} &= \frac{2}{d} \int_0^a \sin \frac{n\pi y}{d} \sin \frac{m\pi y}{a} dy \\ &= \frac{2}{d} \left[\frac{\sin(\frac{n\pi}{d} - \frac{m\pi}{a})a}{\frac{n\pi}{d} - \frac{m\pi}{a}} - \frac{\sin(\frac{n\pi}{d} + \frac{m\pi}{a})a}{\frac{n\pi}{d} + \frac{m\pi}{a}} \right] \end{aligned} \quad (5)$$

Similarly, continuity of the wavefunction derivative at $x = 0$ results in

$$\sum_n C_{1n}^- \alpha_n I_{nm} = \sum_n C_{2n}^- \alpha_n I_{nm} \quad (6)$$

In matrix form, Eqs. (4) and (6) read:

$$C_1^+ = C_2^+ = ID \quad (7)$$

$$I^t \alpha C_1^- = I^t \alpha C_2^- \quad (8)$$

Notice that the above equation does not imply $C_1^- = C_2^-$, since I is not invertible.

Physically, the scattering boundary conditions require that $\overline{C}_2 = 0$ so that no backward wave is traveling in region 2; therefore

$$C_2 = ID \quad \text{and} \quad \overline{C}_1 = ID - C_1. \quad (9)$$

Inserting this into Eq. (8), we obtain

$$D = (I^t \alpha I)^{-1} I^t \alpha C_1 \quad (10)$$

Thus the wavefunction is determined by the injection mode expansion coefficients $C_{1n} = \delta_{nn_i}$.

Calculating the transmission coefficient is not the main purpose of this paper. Rather, we wish to examine how the electron passes through the channel, and to compare this with the corresponding classical motion. To this end, we adopt the formalism of Bohm's interpretation of quantum mechanics [1,2], in which a system is described not only by its wavefunction, but also particle orbits. In this picture, a particle at position \mathbf{r} moves with velocity $\mathbf{v} = \mathbf{j}/|\Psi|^2$, where \mathbf{j} is the probability current density. Since Bohm's picture is most

vividly applied to scattering states, Holland in his recent book called it “the quantum theory of motion” [3]. We are dealing with a time independent wave equation, so the process of finding the particle trajectories is separated from solving for the wavefunction. All we have to do is to find the stream lines of the velocity field deduced from the wavefunction; they are curves tangent to \mathbf{j} .

According to our recent discussion of quantum probability flow [4,5], the stream lines can be classified in three categories: 1) those that close on themselves; 2) those which participate in global transmission, (which start and end at infinity; they could be regarded as special stream lines of type 1 which close at infinity;) 3) those which connect saddle points or end on the boundary; these lines separate different pieces of the flow. In order to study particle transport we concentrate on type 2 stream lines as shown in Fig. 1. We drew these lines by starting from points along the channel opening at $x = 0$, and tracing the trajectories forward and backward. The density of the starting points was taken to be proportional to the probability density in the opening. In order to exhibit the relation to the classical orbits, we deliberately chose a high electron energy. The trajectory in the transmitted region, as expected, clearly resembles that of a classical ball bouncing along between hard walls, or light rays between parallel mirrors. We can understand this better by developing an approximate analytical solution.

Consider a situation where the transverse and longitudinal wave numbers are all large. The computed transmission coefficient is very close to the classical prediction, a/d . A large transverse wave number implies that I_{nm} in Eq. (5) will have appreciable non-zero values only when $n\pi/d \approx m\pi/a$. From this condition and Eq. (10), we see that D_m is concentrated in a narrow interval centering about $m = n_i(a/d)$. Also from Eq. (9), C_{2n} and \overline{C}_{1n} are concentrated about $n = n_i$. These estimates are well verified by exact numerical calculations. Denoting $k_x = \alpha_{n_i}$, $k_y = k_{n_i}$, α_n can be expanded about k_x :

$$\alpha_n - k_x = -(k_n - k_y) \tan \theta \quad (11)$$

where

$$\tan \theta = k_y/k_x \quad . \quad (12)$$

Here we have used the condition of large longitudinal wave number. Under this approximation,

$$\begin{aligned} \Psi_2 &\approx \exp[i(k_x + k_y \tan \theta)x] \times \\ &\quad \sum_n C_{2n} \exp(-ik_n x \tan \theta) \sin(k_n y) \\ &= \exp[i(\alpha_{n_i} + k_{n_i} \tan \theta)x] \times \\ &\quad \sum_n C_{2n} \left[\frac{\cos k_n(y - x \tan \theta) - \cos k_n(y + x \tan \theta)}{2i} \right. \\ &\quad \left. + \frac{\sin k_n(y - x \tan \theta) + \sin k_n(y + x \tan \theta)}{2} \right] \quad . \end{aligned} \quad (13)$$

Expressing $\cos k_n(y \pm x \tan \theta)$ as $(1/k_n)\partial[\sin k_n(y \pm x \tan \theta)]/\partial y$, and approximating $1/k_n = 1/k_y$ in the summation, we obtain

$$\begin{aligned} \Psi_2 &= \exp[i(k_x + k_y \tan \theta)x] \times \\ &\quad \left\{ \frac{1}{2ik_y} \frac{\partial}{\partial y} [\operatorname{sn}(y - x \tan \theta) - \operatorname{sn}(y + x \tan \theta)] \right. \\ &\quad \left. + \frac{1}{2} [\operatorname{sn}(y - x \tan \theta) + \operatorname{sn}(y + x \tan \theta)] \right\} \end{aligned} \quad (14)$$

where the function $\operatorname{sn}(y)$ is defined by Eq. (3), together with its odd symmetry extension, and its periodic extension with period $2d$. In other words,

$$\operatorname{sn}(y) = \begin{cases} \sum_m D_m \sin \frac{m\pi\bar{y}}{a} & |\bar{y}| < a \\ 0 & |\bar{y}| > a \end{cases} \quad (15)$$

where \bar{y} is y minus an integer multiple of $2d$ such that the result falls in $(-d, d]$. Now return to Eq. (14) and consider the derivative of the function $\operatorname{sn}(y)$. Its non-zero part is $\sum_m D_m(m\pi/a) \cos[m\pi\bar{y}/a]$. Now since m is in a narrow region of $n_i a/d$, the factor $m\pi/a$ may be approximated by k_y (this kind of approximation would not be permitted when the factor is inside a rapid changing function such as \sin , \cos , and exponential). This leads to

$$\begin{aligned}
\Psi_2 &\approx \exp[i(k_x + k_y \tan \theta)x] \times \\
&\quad \frac{1}{2i} [\text{cs}(y - x \tan \theta) - \text{cs}(y + x \tan \theta) \\
&\quad + i \text{sn}(y - x \tan \theta) + i \text{sn}(y + x \tan \theta)] \\
&= \exp[i(k_x + k_y \tan \theta)x] \times \\
&\quad \frac{\text{ep}[i(y - x \tan \theta)] - \text{ep}[-i(y + x \tan \theta)]}{2i}
\end{aligned} \tag{16}$$

where

$$\text{cs}(y) = \begin{cases} \sum_m D_m \cos \frac{m\pi\bar{y}}{a} & |\bar{y}| < a \\ 0 & |\bar{y}| > a \end{cases} \tag{17}$$

and

$$\text{ep}(iy) = \text{cs}(y) + i \text{sn}(y). \tag{18}$$

Aside from a phase factor, Eq.(16) expresses Ψ_2 in terms of an exponential-like function $\text{ep}(iy)$. When $x = 0$, it clearly reproduces Eq. (3) since $\text{sn}(y) = [\text{ep}(iy) - \text{ep}(-iy)]/(2i)$. As x increases, $\text{ep}[i(y - x \tan \theta)]$ represents a function $\text{ep}[iy]$ shifted by $x \tan \theta$ upwards, and $\text{ep}[-i(y + x \tan \theta)]$ represents a function $\text{ep}[-iy]$ shifted the same amount downwards. In other words, the two functions $\text{ep}(\pm iy)$ each move at an angle $\pm\theta$ to the channel walls as x increases. The motion of the functions leaves stripes of non-zero parts of the wavefunction. Fig. 2 illustrates the formation of the bouncing ball pattern in between the two thick horizontal lines which represent the wire walls. At the left edge of the figure, vertical line segments locate the non-zero parts of the function $\text{ep}(\pm iy)$. The motion of these vertical lines traces out the upward and downward inclined stripes. What has physical meaning are those portions where the stripes lie inside the wire. Regions marked by a right upward arrow (U-regions) are those due to $\text{ep}(iy)$, and those marked with a right downward arrow (D-regions) are due to $\text{ep}(-iy)$. The triangular regions marked with horizontal arrows (H-regions) are where the two contributions superpose.

Not only can we show that the non-zero part of the wavefunction produces the pattern shown in Fig. 2, we can also show that the trajectories indeed follow the directions shown. To see this we calculate the particle velocity

$$\mathbf{v} = (\hbar/m^*)\text{Im}(\Psi^*\nabla.\Psi)/|\Psi|^2 \quad (19)$$

To compute the gradient of Ψ_2 , first note that

$$\frac{\partial \text{ep}(iy)}{\partial y} = ik_y \text{ep}(iy) \quad (20)$$

in the approximation $m\pi/a \approx k_y$ that we have used before. Thus $\text{ep}(iy)$ behaves much like $\exp(ik_y y)$ in the non-vanishing region. Consider a U-region, where $\Psi_2 = \exp[i(k_x + k_y \tan \theta)x] \text{ep}[i(y - x \tan \theta)]/(2i)$,

$$\frac{\partial \Psi_2}{\partial x} = ik_x \Psi_2, \quad \frac{\partial \Psi_2}{\partial y} = ik_y \Psi_2 \quad (21)$$

which lead to

$$v_x = (\hbar/m^*)k_x, \quad v_y = (\hbar/m^*)k_y; \quad (22)$$

therefore

$$v_y/v_x = \tan \theta. \quad (23)$$

That is to say, the particle moves to the right and upward in a direction determined by the decomposition of the total wave number in the x and y directions. Similarly the particle in a D-region moves in the direction $v_y/v_x = -\tan \theta$.

In an H-region, it is easily seen that v_x takes the same value as in the previous two cases. For v_y , one finds

$$\begin{aligned} \Psi_2^* \frac{\partial \Psi_2}{\partial y} = & ik_y/4 \{ \text{ep}^*[i(y - x \tan \theta)] - \text{ep}^*[-i(y + x \tan \theta)] \} \times \\ & \{ \text{ep}[i(y - x \tan \theta)] + \text{ep}[-i(y + x \tan \theta)] \} \end{aligned} \quad (24)$$

which yields

$$\begin{aligned} \text{Im} \left(\Psi_2^* \frac{\partial \Psi_2}{\partial y} \right) = \\ k_y/4 \left\{ |\text{ep}[i(y - x \tan \theta)]|^2 - |\text{ep}[i(y + x \tan \theta)]|^2 \right\}. \end{aligned} \quad (25)$$

Eq. (25) is a small quantity due to the property of the exponential-like function $\text{ep}(iy)$. The H-regions are symmetrical triangles. Obviously, v_y vanishes when close to the bottom side of the triangle. Along the symmetry line of the triangle, $x \tan \theta = (\text{integer}) \times d$, which implies $|\text{ep}[i(y \pm x \tan \theta)]|$ are equal; thus $v_y = 0$. At other points of these triangles, v_y takes on small values, which allow a smooth connection of the trajectories to the other regions.

So far we have shown clearly the formation of the bouncing ball trajectories in the downstream transmitted region. Let's now discuss the reflected region. From Eq. (1), (9) and $C_{1n} = \delta_{nn_i}$, one has

$$\begin{aligned} \Psi_1 &= e^{ik_x x} \sin(k_n y) + \sum_n (C_{2n} - C_{1n}) e^{-i\alpha_n x} \sin(k_n y) \\ &= 2i \sin(k_x x) \sin(k_n y) + \Psi_2(-x, y) \\ &\equiv \Psi_R + \Psi_2(-x, y) \end{aligned} \quad (26)$$

Here Ψ_R is a standing wave solution for the total reflection problem as if the channel were completely closed at $x = 0$; it represents a standing wave in the upstream or left part of the channel. Thus the complete wave function upstream is a superposition of this standing wave and a reflection of the transmitted wave. The standing wave has a grid of nodal lines which divides the region into cells of size $\Delta x = \pi/k_x$, $\Delta y = \pi/k_y$. The magnitude of the standing wave at the center of each cell is ± 2 . This pattern will be preserved in Ψ_1 at the places not covered by $\Psi_2(-x, y)$. The velocity in these places, however, will be virtually zero since Ψ_R is pure imaginary.

At the places covered by $\Psi_2(-x, y)$, the interference with the standing wave can form quantum vortices [4]. These quantum vortices perturb the stream lines, causing many detours away from straight line trajectories. This is why the trajectories upstream are

much more complex than those downstream in Fig. 1. Quantum vortices appear in many electron waveguide structures, for examples, in that of Lent [6], and Berggren [7].

We now explain the deployment of the quantum vortices. To see a quantum vortex, one must look for an isolated node of the wavefunction, i. e. $\Psi_1/(2i) = \sin(k_x x) \sin(k_y y) + \Psi_2(-x, y)/(2i) = 0$. Thus $\Psi_2(-x, y)/(2i)$ must be real. Writing $\Psi_2(-x, y)/(2i)$ as $R_2 \exp(iS/\hbar)$, we see that the nodes must lie on curves of constant phase $S = \text{integer} \times h/2$. Now $\mathbf{v} = \nabla S/m^*$ would be the velocity if only $\Psi_2(-x, y)$ were present, so constant S curves are orthogonal to \mathbf{v} . Taking a region where the flow is to the right and downward, the orbits are straight lines at an angle $-\theta$ from the horizontal. Thus the constant S curves are also straight lines but at an angle $\pi/2 - \theta$ upward. This is precisely the direction of the upward diagonal line of the standing wave cell. Picking a grid point of the standing wave, $x = -(\pi/k_x)n_x$, $y = (\pi/k_y)n_y$, in the region we are considering now,

$$\begin{aligned} \Psi_2(-x, y)/(2i) &= -(1/4) \exp[i(k_x + k_y \tan \theta) \frac{\pi}{k_x} n_x] \times \\ &\quad \text{ep}[i(\frac{\pi}{k_y} n_y - \frac{\pi}{k_x} n_x \tan \theta)] \end{aligned} \quad (27)$$

Now remembering that $\text{ep}(iy)$ behaves as $\exp(ik_y y)$,

$$\Psi_2(-x, y)/(2i) \approx -R_2 (-1)^{n_x + n_y} \quad (28)$$

which is real on these grid points. Therefore, the constant phase lines allowing quantum vortices are simply the upward diagonal lines of the standing wave cells. The line passing through the grid point (n_x, n_y) is

$$y - \frac{\pi}{k_y} n_y = \tan(\frac{\pi}{2} - \theta) (\frac{\pi}{k_x} n_x + x) = \frac{k_x}{k_y} (\frac{\pi}{k_x} n_x + x). \quad (29)$$

Thus along the upward diagonal line,

$$\sin(k_x x) \sin(k_y y) = (-1)^{n_x + n_y} \sin^2(k_x x). \quad (30)$$

Therefore the condition to find a node is

$$R_2 = \sin^2(k_x x). \quad (31)$$

Of course, the solution will depend on the form of R_2 . Once again, since $\text{ep}(iy) \approx \text{constant} \times \exp(ik_y y)$ in its non-vanishing region, R_2 is a slowly varying function in the said region. Its average value along the diagonal line can be estimated from the transmission coefficient which yields $1/|4 \cos \theta|$, a value normally less than 1. Along the diagonal and within one cell, $\sin^2(k_x x)$ starts from zero at one end, monotonically increases to 1, then monotonically decreases to zero at the other end. Thus one normally sees two vortices per cell along the diagonal direction perpendicular to the average direction of motion of the particle. Fig. 3 shows an array of such cells with two quantum vortices spinning in the opposite directions. The deviations of the vortex centers from the diagonal lines are small. Combined with Fig. 1, one sees that the trajectories *on average* are mirror images of those in the transmitted region which resemble classical trajectories, but in detail they are much more complex. We have therefore found a complete justification for the ballistic trajectory, or the ray optical picture of propagation in the large wave number limit. Corrections to this picture will account for diffraction on both edges of the striped propagation pattern, and slow filling in of the shadow regions on both sides of the classical trajectory. This diffractive effect is seen in Fig. 1, and it is much bigger when the energy is lowered, as seen in Fig. 4. Notice that the average trajectories in the reflected region close to the classical trajectory rely heavily on the fact that the quantum vortices are situated according to the standing wave cell structure. The effect of a small misalignment of quantum vortices may be magnified significantly in the trajectories. This is because there is an equal number of hyperbolic unstable fixed points for each pair of vortices, and these can cause two orbits which are infinitesimally close in one place to follow quite different paths later on. This effect is also seen in Fig. 4.

We would like to add the following additional points of discussion:

- A natural question is, why do we not see turbulence despite the very complex flow pattern? The answer is that we are solving a steady flow problem. By definition, the velocity field does not vary with time. Since the stream lines do not cross each other, a single line can occupy very limited space. However, it would be interesting to see

what would happen if the steady state condition were lifted.

- We have seen that as the energy is lowered, the trajectories start to deviate from the classical ones. An extreme is reached when the energy is so low that there is only one propagating mode. In this case, the wavefunction is well described by the single mode approximation [8] such that the transverse dependence is simply $\sin(\pi y/d)$ except in the region very close to the narrow constriction. Without the phase changing in the y -direction, the stream lines are parallel to the wire. As the stream lines approach the constriction, they will converge so that they may pass through the opening. After escaping, they then relax back and resume their motion parallel to the wire. This situation is common to all devices with straight leads, at low energy.
- Since the stream lines do not cross each other, the bouncing ball trajectories do not really hit the walls. Rather, they turn to a more or less horizontal direction in the H-region(see Fig. 2), to avoid crossing. This is one difference from the strict classical prediction.
- A larger opening width a will enlarge the H-region, and thus lead to stream lines more parallel to the wire as expected.
- Previously we said that on the up-stream side, where not covered by $\Psi_2(-x, y)$, there is no flow motion. This is an approximation. In reality, localized flow circulating in these regions can form quantum vortices, and possibly vortex clusters. This is a typical situation where stream lines close on themselves.
- The problem solved in this paper can be taken as an odd symmetry solution for a wire of width $2d$ with a obstacle placed at its center, which is a variation of the ordinary double slits problem. Or as an odd-symmetry solution for a wire with a constriction standing out from each side of the channel.

In summary, we have given a quantitative description of trajectories in a particular quantum wire transmission problem. The result closely resembles the classical bouncing ball

orbits in the large wave number limit. The major difference lies in the effect of quantum vortices which is responsible for the complex pattern in the up-stream. This simple model can serve as an explicit analytical example of the picture of ballistic transport in quantum waveguides, which in one or another form, clearly or vaguely, exists in our minds.

ACKNOWLEDGMENTS

We are grateful to NSERC Canada for continued support under research grant OGP00-3198.

REFERENCES

- [1] D. Bohm, Phys. Rev. **85**, 166 (1952); **85** 180, (1952).
- [2] D. Bohm, B. J. Hiley, and P. N. Kaloyerou, Phys. Rep. **144**, 321 (1987).
- [3] P. R. Holland, *The quantum theory of motion: an account of the de Broglie-Bohm causal interpretation of quantum mechanics*, (Cambridge University Press, 1993).
- [4] Hua Wu, and D. W. L. Sprung, Phys. Lett. A **183**, 413 (1993).
- [5] Hua Wu, and D. W. L. Sprung, Phys. Rev. A **49**, 4305 (1994).
- [6] C. S. Lent, Appl. Phys. Lett. **57**, 1678 (1990).
- [7] K. F. Berggren, and Z. L. Ji, Phys. Rev. B **47**, 6390 (1993).
- [8] Hua Wu, D. W. L. Sprung, and J. Martorell, Phys. Rev. B **45**, 11960 (1992).

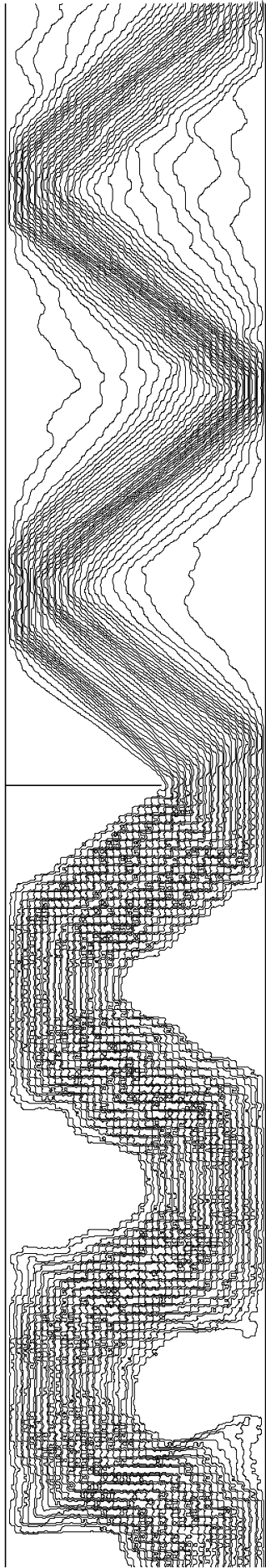
FIGURES

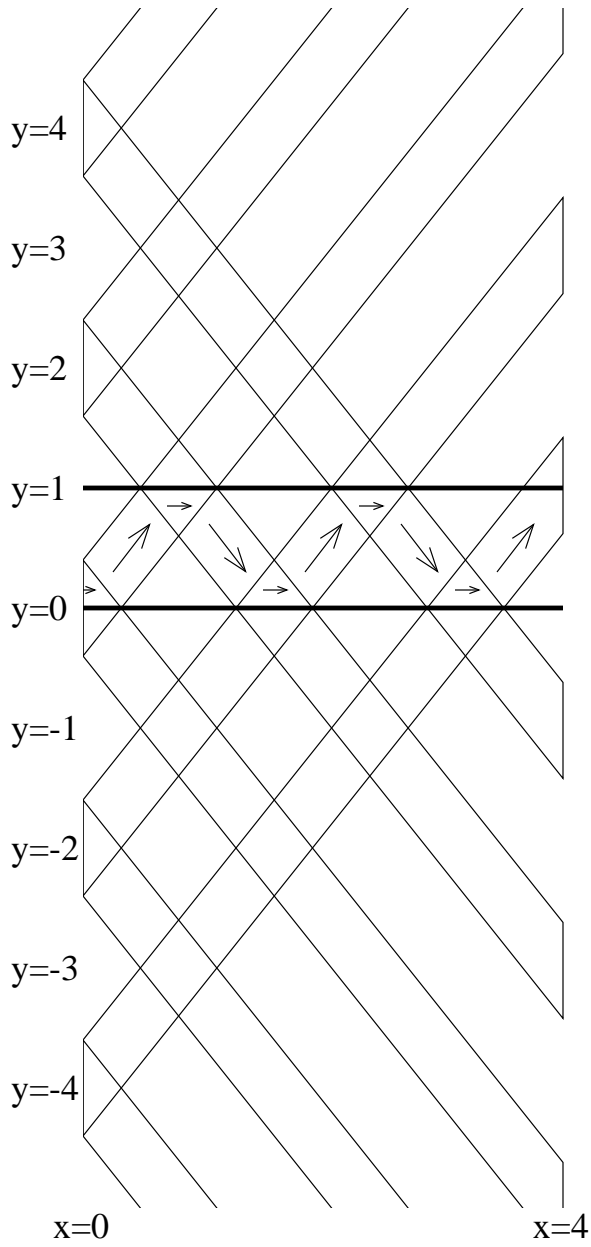
FIG. 1. Stream lines participating in global transmission for a quantum wire with a simple constriction. $a = 0.4d$, $E = 50.5^2(\pi/d)^2$, $n_i = 40$. The angle θ reduced is 52.4° .

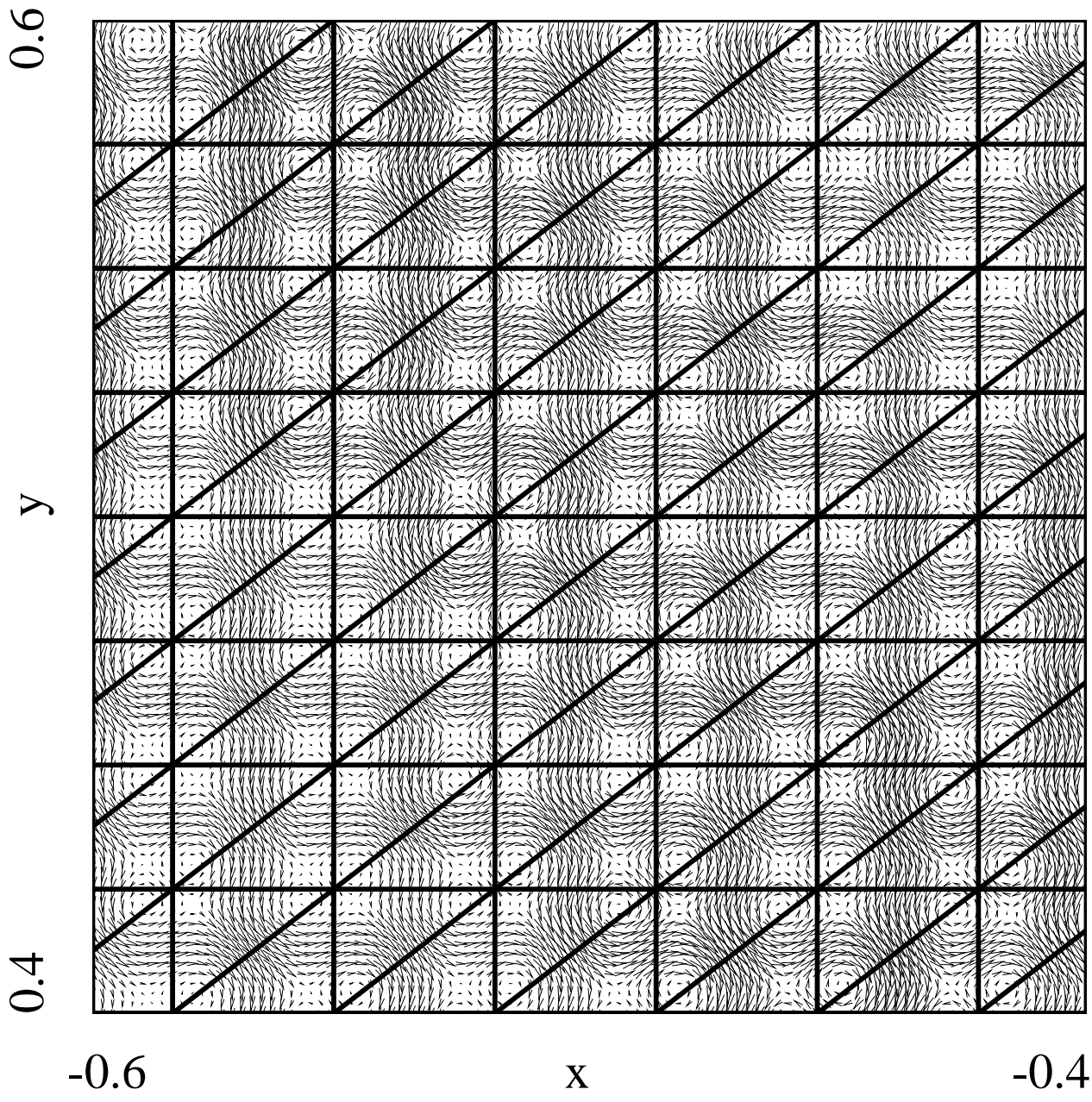
FIG. 2. Formation of the bouncing ball pattern in the transmitted region due to the shift of the function $\text{ep}(\pm iy)$ as x increases.

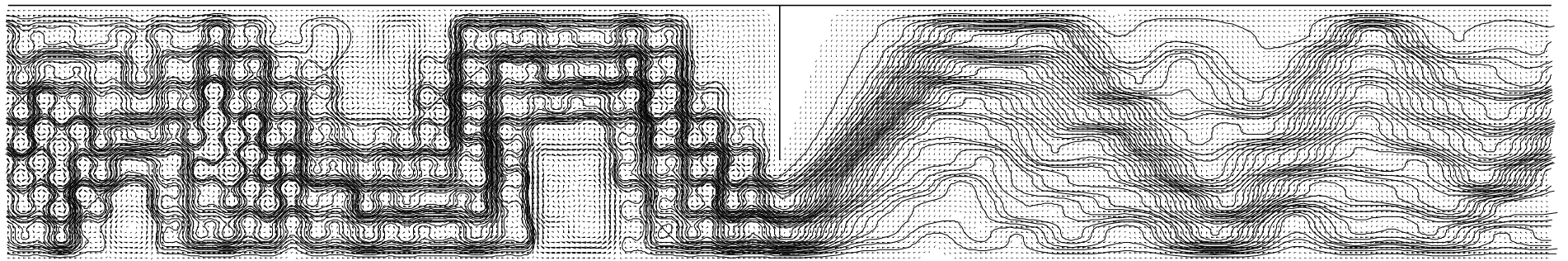
FIG. 3. Current density plot in a portion of the up-stream propagating region. The grid standing wave pattern and associated quantum vortices are clearly seen. Horizontal and vertical lines are standing wave node lines. Inclined diagonal lines are the theoretical constant phase lines where $\Psi(-x, y)/(2i)$ is real. Parameters are the same as Fig. 1.

FIG. 4. Same as Fig. 1 but at a lower energy: $E = 10.5^2(\pi/d)^2$, $n_i = 8$.









$x = -3d$

$x = 0$

$x = 3d$